CrystEngComm

View Online
Dynamic Article Links

Cite this: *CrystEngComm*, 2011, **13**, 5818

www.rsc.org/crystengcomm

PAPER

On the reversed crystal growth of $BaZrO_3$ decaoctahedron: shape evolution and mechanism

Mário L. Moreira,*[a] Juan Andrés,[b] Valmor R. Mastelaro,[c] José A. Varela[a] and Elson Longo[a]

Received 25th March 2011, Accepted 23rd June 2011
DOI: 10.1039/c1ce05361b

$BaZrO_3$ (BZO) nanoparticles were nucleated, grown and subsequently self-assembled into a 3D decaoctahedronal architecture *via* a microwave-assisted hydrothermal (MAH) method. X-Ray diffraction (XRD), field emission scanning microscopy (FE-SEM), X-ray absorption spectroscopy (XAFS) as well as both photoluminescence (PL) and radioluminescence (RL) emission studies have provided fundamental insight into the nature of the anisotropic crystal growth mechanism of BZO nanocrystals into their final decaoctahedral shape. The growth mechanism of the assembled nanoparticles *via* mesoscale transformations to form BZO decaoctahedrons occurs from the surface to the core along a reversed crystallization route. This pathway is accompanied by a large enhancement of RL emissions while the intensity of PL emissions is enhanced and worsened along the process. The analysis of the results reveals a relationship between the decaoctahedrons obtained and their optical properties.

Introduction

A deep understanding of the formation process, crystal growth mechanism and key factors which determine the shape and size of these materials is crucial for a rational design and controlled synthesis.[1–8] It is essential to establish the sequence of events involved in the growth mechanism, rather than simply studying the morphological and structural properties of the bulk crystals collected at the end of the process. It is very difficult to establish how crystals actually evolve during growth by applying experimental techniques for a wide range of reasons; *e.g.*, due to limitations arising from the crystallization apparatus, the specific experimental conditions required or the time scales involved.[9–17] Solution-based synthesis approaches are the most widely adopted "bottom-up" strategies, which enable the precise control of the nanocrystals size, shape and composition of nanocrystals during the growth process and hence the ability to tailor their properties at the nanoscale size.[18–22] Considerable knowledge has evolved regarding a general understanding of the nucleation and growth processes in solution; however, the crystal structure prediction resulting from a specific reaction is still elusive. Patzke *et al.*[23] have been reviewed synthetic developments and technological innovations for oxide nanomaterials production.

In a solution-based synthesis, nanocrystal growth processes are controlled mainly by two distinct mechanisms: Ostwald ripening (OR) and oriented attachment (OA). OR is commonly referred to as the solution progress where larger grains grow at the expense of smaller grains with relatively higher solubility,[24,25] while the OA involves the spontaneous self-organization of adjacent particles which share a common crystallographic orientation and join together at a planar interface.[26–28]

Crystal growth *via* OA or OR often exhibits exclusive features. Compared to classical OR, OA growth is based on the separation of the nucleation and the subsequent growth process,[29,30] which provides a deeper understanding of the growth process of nano- and mesocrystals to some extent. The OR mechanism normally produces nanoparticles with regular shapes and few defects while the OA mechanism usually results in nanoparticles with irregular morphologies and typical defects such as twins, stacking faults and orientation loss.[26,31] The essence of the OA mechanism is that small nanocrystals with a common crystallographic orientation aggregate and form larger ones.[32]

The attachment of these primary nanoparticles is irreversible and occurs in a highly oriented manner, leading to the elimination of the interfaces of joint crystals. Thus, the reduction of the surface energy and the increase in entropy serve as the driving forces for the OA growth process. In general, OR and OA are regarded as two independent and competitive processes. However, they could coexist simultaneously under certain conditions for the hydrothermal growth of nano- and microcrystals.[33] Recently, the assembly of nanocrystalline building blocks into single-crystal or other complex architectures *via* an

[a]*INCTMN, Department of Physical Chemistry, Institute of Chemistry, Unesp—Universidade Estadual Paulista, Prof. Francisco Degni Street, s/n°, Quitandinha, Araraquara, SP, 14800-900, Brazil. E-mail: mlucio@liec.ufscar.br; mlucio3001@gmail.com; Fax: +55 16 3351 8214; Tel: +55 16 3351 8214*
[b]*Departament de Química Física i Analítica, Universitat Jaume I, Campus de Riu Sec, Castelló, E-12080, Spain*
[c]*Instituto de Física de São Carlos, USP, PO Box 369, 13560-970 São Carlos, SP, Brazil*

OA growth process can be considered as one of the most interesting fields in nanoscience.[34–39] In particular, Zhang *et al.*[40] reviewed recent advances in the oriented attachment growth and synthesis of functional materials while Leite *et al.*[41] have been published a new concept of the OA mechanism regarding achievement of the self-organization or mutual orientation of adjacent nanocrystals.

Very recently, Zhou[42] presented a general mechanism for an innovative crystal growth process, reversed crystallization. This reversed process consists of three well defined stages: (1) aggregation of nanoparticles, (2) surface crystallization followed by (3) surface-to-core extension of recrystallization. Evidence of such novel crystal growth phenomenon has been found in materials such as zeolites and $CaTiO_3$ perovskite.[43–48] However, this mesoscale transformation process and its mechanism are still challenging because current interests are more focused on the investigation of its role rather than on comprehensive insight into the mechanism. Concomitant mechanisms lead to increased difficulty in understanding this growth process, which is important and must be the focus of detailed studies of the nanocrystal growth mechanism.

In earlier reports, we used the microwave-assisted hydrothermal method for the synthesis of semiconducting oxide nanomaterials which exhibited excellent electronic and optical properties. We have selected this procedure because it provides an environmental method of heating for the generation of nanomaterials which combines effects of solvent, temperature, and pressure on ionic reaction equilibrium,[49–51] and represents a major step toward a green-chemistry approach for the synthesis of high-quality nanoparticles. In this context, we present the case of a reversed crystal growth mechanism for the formation of $BaZrO_3$ (BZO) nanograins, to achieve a further understanding of this mechanism. The changes on the morphology of BZO samples during the synthesis time have been investigated by exploring the nanocrystal growth mechanism followed by the assembled process into microcrystals shaped *via* reversed crystallization. An examination of the acquired samples using complementary characterization techniques such as XRD, FE-SEM, X-ray absorption spectroscopy (XAFS), as well as both PL and RL emissions has provided fundamental insight into the nature and anisotropic crystal growth mechanism of BZO nanocrystals.

Methodology

BZO products were synthesized using two different chloride precursors: (1) zirconyl chloride octahydrate $ZrOCl_2\ 8H_2O$ (99.50%, Aldrich) at 0.01 M and (2) barium chloride dihydrate $BaCl_2\ 2H_2O$ (99,90%) at 0.01 M. Both precursors were dissolved in double de-ionized water at 50 °C into a Teflon® vessel which were co-precipitated by 6 M of KOH (Merck) under constant agitation. The solution containing the precipitates was placed into a sealed autoclave of the MAH system which applies 2.45 GHz of microwave radiation with a maximum output power of 800 W. The reaction mixture was heated to 140 °C in less than 1 min (at 800 W) by a direct interaction between water molecules and microwave radiation and kept at this temperature for 10 (BZO10), 20 (BZO20), 40 (BZO40), 80 (BZO80) and 160 (BZO160) minutes under a pressure of 2.5 bar. The autoclave was ambiently cooled to room temperature, and the solid product was washed with de-ionized water until a neutral pH was reached and then dried at 80 °C for 12 h.

Results and discussions

A series of intermediate specimens produced during the crystal growth were collected and investigated to understand the formation mechanism of the reversed crystallization process (see Fig. 1). The BZO decaoctahedron size decreases from 2.3 μm for BZO10 to 1.8 μm for BZO160, showing a typically densification process.

An analysis of Fig. 1 points out that the growth mechanism comprises the generation of near-spherical superstructures by a typical assembly process for BZO10 and BZO20 samples. With the hydrothermal treatment assisted by microwave radiation, the dispersed nanoparticles aggregate as spherical-like superstructures which are not hollow spherical particles (see Fig. 1a,

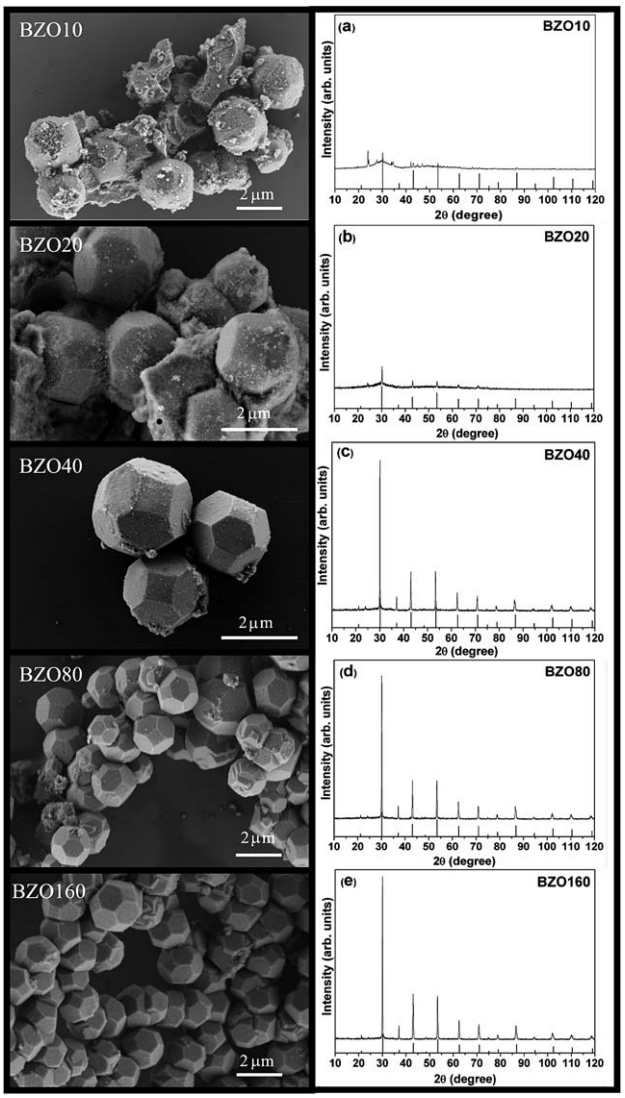

Fig. 1 BZO X-ray diffractions following crystallization evolution at (a) 10, (b) 20, (c) 40, (d) 80, and (e) 160 min with their respective FE-SEM images.

FE-SEM), indeed are composed of self-assembled nanoparticles in a mesoscale system (see Fig. 2a). Based on diffraction patterns of Fig. 1, it is clear that the BZO10 sample does not correspond to a well crystallized BZO phase, instead it almost exhibits two different poorly crystallized phases even at BZO20. Barium carbonate, $BaCO_3$ with JCPDS card no. 05-0378, and tetragonal ZrO_2 were identified in BZO10 diffractions. The tetragonality of ZrO_2 probably is a consequence of reduced size of the assembled nanoparticles shown in Fig. 1(a) and (b). Several structural modifications have been reported in the literature as a consequence of the introduction of dopants and/or temperature increases. In this respect, it is important to note that these chemical manipulations on different perovskites showed very significant improvements in their ferroelectric properties.[52] It was decided that the hydrothermal heat treatment time should be prolonged. Hence, the assembled nanoparticles start to crystallize in the pure BZO phase with a decaoctahedral shape, identified by JCPDS card no. 06-0399.

From the analysis of the results, we can propose that the resulting temperature of the heating medium (water) is transferred to the aggregate of nanoparticles more effectively from the surface to the core. Likewise, the crystallization process at the inward moiety will be slower than at the surface; thus, through a mesoscale transformation, the surface energy will be minimized by forming a shell oriented at the {110} direction as estimated by TEM micrographs of Fig. 2. In other words, at a very early stage of crystal growth, there is a competition between the aggregation and growth processes for BZO nanoparticles. If crystal growth is rapid, individual crystallites quickly approach a certain size, where aggregation is difficult (classical OR mechanism).[24,25,41] If aggregation occurs before the crystals become too large due to a strong van de Waals interaction between them,[50] the crystal growth of individual crystallites is suppressed in favour of the reversed crystallization process. Furthermore, the affinity of KOH solutions with the shell formed by previously assembled nanoparticles favours the starting crystallization from the outer surfaces to the core. The BZO nanoparticles assembly process is followed by a pseudo core–shell growth as described above (see Fig. 3). In a cluster of nanoparticles, fewer, however larger crystals may be created, which have smaller surface-to-volume ratios if compared to others with only small particles, thus reducing the energy of the entire system. When the reaction time is prolonged, the microsphere surface recrystallizes into a kind of single crystalline shell, and the polyhedral morphology is gradually developed.

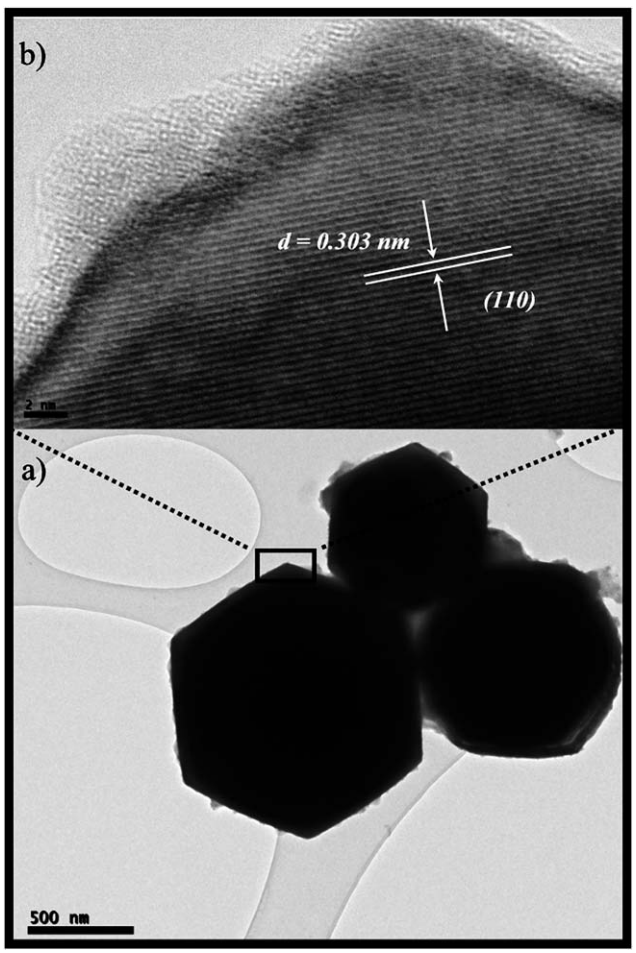

Fig. 2 Transmission images at the corner of BZO decaoctahedrons shell growth in the {110} direction.

Cubic BZO crystals usually expose {110} faces which present a lower surface energy[53] is in agreement with the results reported in the observed HR-TEM image of Fig. 2. However, the crystal morphology depends not only on the intrinsic crystal structure, but also on synthesis conditions. As the nanoparticle size increases, the surface energy minimization followed by BZO phase formation is associated with the shell growth; giving rise to the reversed crystallization process as detected from the BZO20 sample. Possibly, this shell originates from recrystallization of the outer part of the spherical-like aggregates at the expense of the inner part, which acts as a seminal material. The inner part of the assembly is naturally low ordered and/or composed of smaller primary nanocrystals, as depicted in the schematic diagram of Fig. 3. It is important to note that in the morphologies reported in Fig. 1 and 3, both final size and shape are practically the same: however the broken particles shown in Fig. 3 are slightly distorted as expected.

The nanoparticles exposed by the broken particle in Fig. 3b are bound by the walls of the shell. The nanoparticle size shell can act as a material source to start the growth process which yields a faceted superstructure under the decaoctahedral shape. These particles can also be washed out to produce hollow decaoctahedrons (see Fig. 3a and c) with micrometric final size, providing the driving force for the crystallization process of shells under decaoctahedral shape. These grains (decaoctahedrons) consist of highly defective primary crystals, with a large amount of holes clearly present on the shells mainly until BZO40 (Fig. 1c). These interstitial holes may provide channels to produce larger interior cavities *via* an OR mechanism, which after 40 min (BZO40) of annealing treatment are almost completely suppressed with a smooth surface (BZO80).

Because pseudo core–shell microspheres have been formed initially in our experiment, the low concentration of the growth nutrients would be insufficient for faces to grow perfectly in the following dissolving–recrystallizing process. Furthermore, during the process, the size of the particles changes only slightly, which is confirmed by the FE-SEM images of the products obtained at different reaction times. Therefore, BZO microcrystals with polyhedral morphology were ultimately formed as

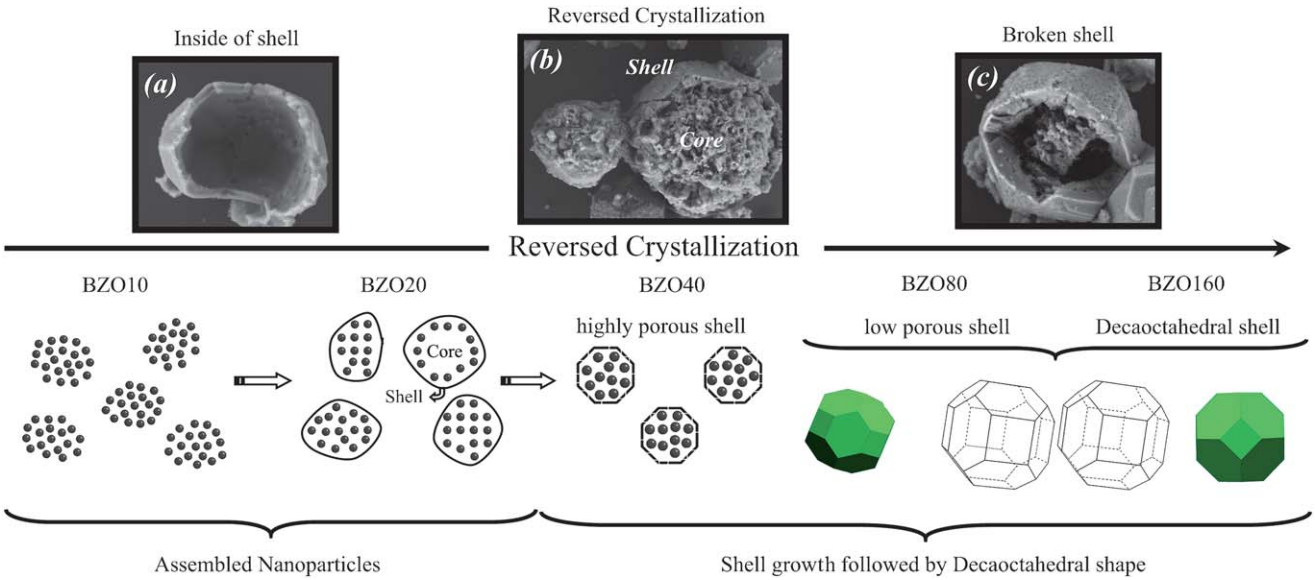

Fig. 3 FE-SEM images of broken decaoctahedrons illustrating the reversed crystallization process associated with a schematic diagram of BZO decaoctahedron formations at different synthesis times, from 10 (BZO10) until 160 min (BZO160).

a result of previously grown nanoparticles which self-assembled into a decaoctahedral super-structure *via* a reversed crystallization process. In this sense the BZO well crystallized decaocthahedrons as BZO40, BZO80 and BZO160 always show a hexagonal shape for bright field transmission images regardless of crystal orientation.

Optical properties are strongly dependent upon the structural and morphological features of the crystal system. Among these factors, the structural order–disorder effects associated with sizes, surface states and lattice defects are invoked as a crucial factor in determining the PL and RL of the material. In fact, both the surface states and lattice defects are closely related to crystal growth mechanisms, and the luminescence mechanism of both PL and RL emissions is different during synthesis times. When the classic OR growth mechanism is involved, nanocrystals are inclined to have relatively regular lattices, making the variation of the surface defects the main factor influencing luminescent properties. However, when the OA mechanism is dominant, the nanocrystals may generally contain a large number of internal lattice defects. Since the OA and OR mechanisms coexist during nanosynthesis, difficulties arise in the investigation of the relationship between luminescence properties and defect states.

Different research groups have found that PL intensities are directly related to several oxides through its particle sizes.[54,55] However, comprehensive knowledge about how to control the formation and disappearance of order–disorder effects is not available. Therefore, we have employed PL and RL emissions to investigate the relationships between optical properties and growth evolution of the system (see Fig. 4). In that case the PL intensity increases if the particle size decreases as a result of quantum effects and surface defects introduced. In our research, clear relationships between size and luminescence emissions were identified. Firstly the PL intensity increased until BZO40 sample and then decrease back to the initial intensity (Fig. 4) which can be associated with the degree of structural order–disorder defects during the reversed crystallization process.[50] Nevertheless, the scintillation associated with RL emission is not as sensitive to these subtle relationships of order–disorder along the crystal growth evolution, and in this case, only defects caught within the band gap of the crystalline compound can effectively participate in the process.[8]

To understand the correlation between the luminescence properties and the formation process, we employed the concept of constituent polyhedral clusters as structural motifs. Using the BZO as a representative perovskite material, the constituent clusters are the sixfold [ZrO_6] and twelvefold [BaO_{12}].[50] Ideal bulk materials of infinite size without any defect, edge or impurity are formed by these clusters. Based on both experimental and theoretical calculations performed by our group, we have shown that PL emission in perovskite based materials originates mainly from their structural disorder in the short-range order of these clusters.[49,56,57] During the PL process the long-range order that characterizes a crystalline structure remains. However, for the initial samples a symmetry breaking process occurs at short order, involving two clusters; *i.e.*, structural distortions associated with imperfect coordination of Zr and Ba sites. Then, the full coordination of the material disappears and the under-coordination associated with the presence of distorted [ZrO_5] and [BaO_{11}] clusters appears. This imperfection is distributed randomly in the lattice, and BZO10 and BZO20 samples are good examples to the situation that this effect is predominant. Moreover, if only a few distorted clusters remain, the BZO160 sample provides the most appropriated representation.

From a structural and electronic standpoint, the optical transition involved in PL measurements is due to a reorganization of electronic charges in distorted [ZrO_6] and [BaO_{12}] clusters in the BZO material. Distorted clusters yield a lattice distortion that is propagated throughout the material, shifting the surrounding clusters away from their ideal positions. Thus, distorted clusters must move for these properties to occur, changing the electronic distribution throughout the network of these polar clusters. These movements can be induced within the crystal

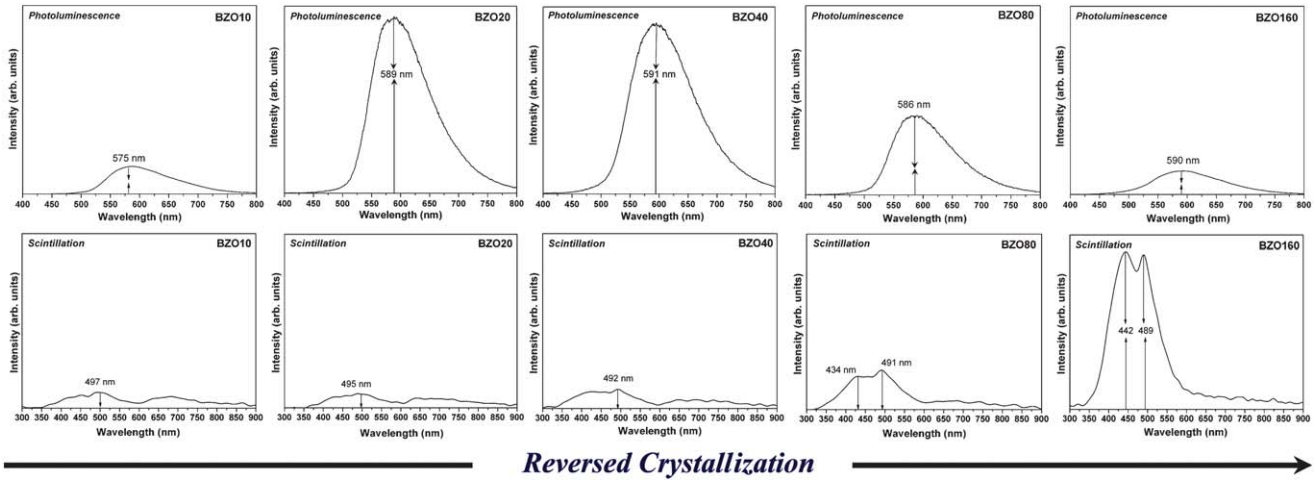

Fig. 4 Scintillation and photoluminescence behavior of the undoped BZO system along the synthesis time evolution.

lattice by irradiation during the measurements, and this anisotropic cooperative movement leads to the PL property. This line of reasoning is similar to the proposal of Sun[58] based on the dominance of broken bonds and non-bonding electrons at the nanoscale level. From recent theoretical calculations, we are able to characterize the excited electronic states where the presence of atomic under-coordination related to distorted [ZrO_5] and [BaO_{11}] clusters is the key ingredient.[57]

Conversely, to obtain a significant RL emission, many factors should be considered as the high periodic order that must be achieved to form the cubic BZO system. Consequently, an alternative technique such as XAFS has been used to characterize these samples; XAFS was performed to better understand the influence of the local order on optical properties. In fact, these techniques provide information on the local order and coordination environment of Zr. In particular, the height of Zr L_{III}-edge features has been shown to be related to the geometry of Zr-oxygen polyhedra, *i.e.*, clusters. Our experimental observations suggest that the XANES region is highly sensitive to disorder in the short- and medium-range environment of the Zr center which is associated with distorted clusters. Therefore, any change in the environment that alters the electronic structure of the absorbing atom should be reflected in the results and can be related to the corresponding optical properties. A theoretical interpretation of these results (Fig. 5) together with a general discussion of the effects of order–disorder is also given. The Zr L_{III}-edge of BZO is characterized by two main distinctive features (A and B) that correspond to split between the signals of orbitals t_{2g} and e_g situated in the Zr edge. The separation of t_{2g} and e_g orbitals is related to electronic transitions from the occupied O 2p orbitals to the empty Zr 4d orbitals.[59] In oxides, the relative intensity of the A and B peaks depends strongly on the chemical environment around the Zr cations.[59] In the temperature that the spectra were acquired (25 °C), a cubic structure is the thermodynamically stable phase for BZO[50] as shown in Fig. 1. Moreover, from the viewpoint of the Zr local symmetry, only BZO160 shows a highly ordered ZrO_6 octahedron into cubic structure[60] because the relative intensity between A and B peaks is clearly stronger than the relative intensity observed for any other symmetries. A careful analysis of Fig. 5 also shows that the separation of peaks A and B for the other samples is not so clear, which does not confirm the existence of well-ordered ZrO_6 clusters for these samples.

From the results presented in Fig. 1, 4 and 5 aided by previous studies on order–disorder effects, scintillation requirements (RL emissions) and fine structural absorptions, only the BZO160 sample presents a local and long range order. Thus, we propose that the origin of RL increasing emissions for the BZO system at room temperature is related to the frozen disorder at medium range in the samples. Then, the reversed crystallization process is able to eliminate short and long range defects, although it is unable to eliminate all medium range defects in BZO crystals. When the reversed crystallization is completed, the inner part of the decaoctahedron is crystallized and all ZrO_6 clusters are formed, however, a minimal amount of defects remain in the lattice as a result of reversed crystal growth.

Very recently, Zhou *et al.*[61] discovered a novel phenomenon consisting of a reversed direction of crystal growth when preparing zeolite analcime; meanwhile, a surface-to-core

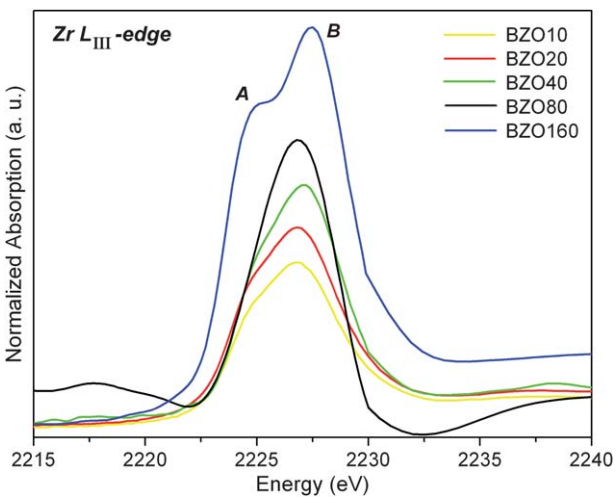

Fig. 5 X-Ray absorption spectroscopy applied to investigate the local symmetry of the zirconium L_{III}-edge into the BZO cubic lattice at different times.

crystallization of zeolite A was observed by Wang *et al.*[44] Based on these observations, a reversed crystal growth route is proposed.[42] The present work may provide indirect evidence for such crystal growth route which would be surely beneficial to the design and fabrication of perovskite-based materials.

Conclusions

This work summarizes recent advances in the controlled growth of $BaZrO_3$ crystals to nano-, meso and microcrystals *via* MAH method. Different experimental techniques have provided fundamental insight into the anisotropic crystal growth providing temporal 'snapshots' of the reaction products formed during the synthesis.

The main results can be summarized as follows: (i) at the early stages of crystal growth, the OA can assist the nanoparticle aggregation process, and OR mechanisms may not be operative; (ii) the second step is surface crystallization with the {110} preferential direction, and then extension from surface to core of the disordered aggregates; (iii) a well defined polyhedral morphology can be reached in a thin surface crystalline layer of a particle with a disordered core; (iv) from this point the OR mechanisms can help in the thickening of the shell; (v) results suggest that the anisotropic crystal growth mechanism of BZO nanocrystals plays an important role in determining the extent to which changes in PL and RL occur; (vi) a theoretical model based on the presence of uncoordinated bonds and/or charge distribution in the distorted constituent clusters (ZrO_6) and (BaO_{12}) of the material can be related to the change in both surface and internal defects during crystal growth. The present work on the formation of BZO nanocrystals may provide indirect evidence for a case of reversed crystal growth route and would be surely beneficial to the design and fabrication of different materials, and can be applied to hollow crystals growth *via* hydrothermal synthesis.

Acknowledgements

This work is supported by FAPESP/CEPID 98/14324-8, CNPq, and national institutions INCTMN and INAMI. J.A. acknowledges to *Ministerio de Educación y Cultura* (project CTQ2009-14541-C02) of the Spanish Government, PROMETEO program (PROMETEO/2009/053) of the Generalitat Valenciana, and Programa de Cooperación Científica con Iberoamerica (Brazil), *Ministerio de Educación* (PHB2009-0065-PC), Thanks for scientific support to Prof. M. S. Li (Physical Institute of USP-São Carlos) and technical support of Rorivaldo Camargo and Madalena Tursi. Thanks for XANES - D04A - SXS facilities provided by LNLS, Campinas, Brasil.

References

1 H. Colfen and S. Mann, *Angew. Chem., Int. Ed.*, 2003, **42**, 2350.
2 J. X. Huang, Y. Xie, B. Li, Y. Liu, Y. T. Qian and S. Y. Zhang, *Adv. Mater.*, 2000, **12**, 808.
3 R. C. Jin, Y. W. Cao, C. A. Mirkin, K. L. Kelly, G. C. Schatz and J. G. Zheng, *Science*, 2001, **294**, 1901.
4 J. Y. Lao, J. G. Wen and Z. F. Ren, *Nano Lett.*, 2002, **2**, 1287.
5 X. Peng, L. Manna, W. Yang, J. Wickham, E. Scher, A. Kadavanich and A. P. Alivisatos, *Nature*, 2000, **404**, 59.
6 H. Shi, L. Qi, J. Ma and H. Cheng, *J. Am. Ceram. Soc.*, 2003, **125**, 3450.
7 Y. Xie, J. X. Huang, B. Li, Y. Liu and Y. T. Qian, *Adv. Mater.*, 2000, **12**, 1523.
8 M. L. Moreira, D. P. Volanti, J. Andrés, P. J. R. Montes, M. E. G. Valerio, J. A. Varela and E. Longo, *Scr. Mater.*, 2011, **64**, 118.
9 F. Rey, G. Sankar, J. M. Thomas, P. A. Barrett, D. W. Lewis, C. R. A. Catlow, S. M. Clark and G. N. Greaves, *Chem. Mater.*, 1995, **7**, 1435.
10 G. Sankar, J. M. Thomas, F. Rey and G. N. Greaves, *J. Chem. Soc., Chem. Commun.*, 1995, 2549.
11 C. A. Koh, J. L. Savidge and C. C. Tang, *J. Phys. Chem.*, 1996, **100**, 6412.
12 M. D. Hollingsworth, M. E. Brown, A. C. Hillier, B. D. Santarsiero and J. D. Chaney, *Science*, 1996, **273**, 1355.
13 M. D. Ward, *Chem. Rev.*, 2001, **101**, 1697.
14 H. Groen and K. J. Roberts, *J. Phys. Chem. B*, 2001, **105**, 10723.
15 C. E. Hughes and K. D. M. Harris, *J. Phys. Chem. A*, 2008, **112**, 6808.
16 M. Shoaee, M. W. Anderson and M. P. Attfield, *Angew. Chem.*, 2008, **120**, 8853.
17 M. Bremholm, M. Felicissimo and B. B. Iversen, *Angew. Chem.*, 2009, **121**, 4882.
18 A. R. Tao, S. Habas and P. Yang, *Small*, 2008, **4**, 310.
19 X. Wang and Y. Li, *Chem. Commun.*, 2002, 764.
20 S. Hu and X. Wang, *J. Am. Ceram. Soc.*, 2008, **130**, 8126.
21 A. Nisar, J. Zhuang and X. Wang, *Chem. Mater.*, 2009, **21**, 3745.
22 P.-p. Wang, B. Bai, S. Hu, J. Zhuang and X. Wang, *J. Am. Ceram. Soc.*, 2009, **131**, 16953.
23 G. R. Patzke, Y. Zhou, R. Kontic and F. Conrad, *Angew. Chem., Int. Ed.*, 2010, **50**, 826.
24 M. V. Speight, *Acta Metall.*, 1968, **16**, 133.
25 C. Wagner, *Z. Elektrochem.*, 1961, **65**, 581.
26 R. L. Penn and J. F. Banfield, *Science*, 1998, **281**, 969.
27 Z. Y. Tang, N. A. Kotov and M. Giersig, *Science*, 2002, **297**, 237.
28 Z. L. Wang, *J. Phys. Chem. B*, 2000, **104**, 1153.
29 R. L. Penn and J. F. Banfield, *Geochim. Cosmochim. Acta*, 1999, **63**, 1549.
30 J. F. Banfield, S. A. Welch, H. Zhang, T. T. Ebert and R. L. Penn, *Science*, 2000, **289**, 751.
31 F. Huang, H. Zhang and J. F. Banfield, *J. Phys. Chem. B*, 2003, **107**, 10470.
32 J. Zhang, F. Huang and Z. Lin, *Nanoscale*, 2010, **2**, 18.
33 F. Huang, H. Zhang and J. F. Banfield, *Nano Lett.*, 2003, **3**, 373.
34 C. Schliehe, B. H. Juarez, M. Pelletier, S. Jander, D. Greshnykh, M. Nagel, A. Meyer, S. Foerster, A. Kornowski, C. Klinke and H. Weller, *Science*, 2010, **329**, 550.
35 V. M. Yuwono, N. D. Burrows, J. A. Soltis and R. L. Penn, *J. Am. Ceram. Soc.*, 2010, **132**, 2163.
36 W.-k. Koh, A. C. Bartnik, F. W. Wise and C. B. Murray, *J. Am. Ceram. Soc.*, 2010, **132**, 3909.
37 G. Xi and J. Ye, *Inorg. Chem.*, 2010, **49**, 2302.
38 G. Zhang, W. Wang, X. Lu and X. Li, *Cryst. Growth Des.*, 2008, **9**, 145.
39 T. Tsuruoka, S. Furukawa, Y. Takashima, K. Yoshida, S. Isoda and S. Kitagawa, *Angew. Chem., Int. Ed.*, 2009, **48**, 4739.
40 Q. Zhang, S.-J. Liu and S.-H. Yu, *J. Mater. Chem.*, 2009, **19**, 191.
41 C. J. Dalmaschio, C. Ribeiro and E. R. Leite, *Nanoscale*, 2010, **2**, 2336.
42 W. Zhou, *Adv. Mater.*, 2010, **22**, 3086.
43 X. Chen, M. Qiao, S. Xie, K. Fan, W. Zhou and H. He, *J. Am. Ceram. Soc.*, 2007, **129**, 13305.
44 J. Yao, D. Li, X. Zhang, C.-H. Kong, W. Yue, W. Zhou and H. Wang, *Angew. Chem., Int. Ed.*, 2008, **47**, 8397.
45 X. Yang, J. Fu, C. Jin, J. Chen, C. Liang, M. Wu and W. Zhou, *J. Am. Ceram. Soc.*, 2010, **132**, 14279.
46 Z. Wang, Y. Liu, J.-G. Jiang, M. He and P. Wu, *J. Mater. Chem.*, 2010, **20**, 10193.
47 E.-P. Ng, L. Itani, S. S. Sekhon and S. Mintova, *Chem.–Eur. J.*, 2010, **16**, 12890.
48 Z. Wang, Y. Liu, J.-G. Jiang, M. He and P. Wu, *J. Mater. Chem.*, 2010, **20**, 10193.
49 L. R. Macario, M. L. Moreira, J. Andres and E. Longo, *CrystEngComm*, 2010, **12**, 3612.
50 M. L. Moreira, J. Andres, J. A. Varela and E. Longo, *Cryst. Growth Des.*, 2009, **9**, 833.

51 F. V. Motta, R. C. Lima, A. P. A. Marques, E. R. Leite, J. A. Varela and E. Longo, *Mater. Res. Bull.*, 2010, **45**, 1703.
52 D. Pontes, E. Longo, F. Pontes, M. Galhiane, L. Santos, M. Pereira-da-Silva, J. da Silva, A. Chiquito and P. Pizani, *Appl. Phys. A: Mater. Sci. Process.*, 2009, **96**, 731.
53 A. V. Bandura, R. A. Evarestov and D. D. Kuruch, *Surf. Sci.*, 2010, **604**, 1591.
54 D. Kan, T. Terashima, R. Kanda, A. Masuno, K. Tanaka, S. Chu, H. Kan, A. Ishizumi, Y. Kanemitsu, Y. Shimakawa and M. Takano, *Nat. Mater.*, 2005, **4**, 816.
55 A. Zhang, M. Lü, S. Wang, G. Zhou, S. Wang and Y. Zhou, *J. Alloys Compd.*, 2007, **433**, L7.
56 V. M. Longo, M. das GraAa Sampaio Costa, A. Z. SimAes, I. L. Viana Rosa, C. O. Paiva Santos, J. AndrAs, E. Longo and J. A. Varela, *Phys. Chem. Chem. Phys.*, 2010, **12**, 7566.
57 L. Gracia, J. Andrés, V. M. Longo, J. A. Varela and E. Longo, *Chem. Phys. Lett.*, 2010, **493**, 141.
58 C. Q. Sun, *Nanoscale*, 2010, **2**, 1930.
59 P. Li, I. W. Chen and J. E. Penner-Hahn, *Phys. Rev. B: Condens. Matter*, 1993, **48**, 10074.
60 W. Xianqin, C. H. Jonathan, A. R. Jose, B. Carolina and F.-G. Marcos, *J. Chem. Phys.*, 2005, **122**, 154711.
61 H. Greer, P. S. Wheatley, S. E. Ashbrook, R. E. Morris and W. Zhou, *J. Am. Ceram. Soc.*, 2009, **131**, 17986.

